



Cite this: DOI: 10.1039/d6cc01700b

 Received 20th March 2026,  
Accepted 18th May 2026

DOI: 10.1039/d6cc01700b

[rsc.li/chemcomm](https://rsc.li/chemcomm)

## Topotactic conversion of Ni<sub>3</sub>CuN into Ni<sub>3</sub>Cu with anti-perovskite structure reveals the role of nitrogen on electrocatalytic properties

 Zhengxin Yang, Angela Daisley,  Christopher Kelly, Justin S. J. Hargreaves  and Alexey Y. Ganin \*

**A topotactic route from anti-perovskite Ni<sub>3</sub>CuN into phase-pure Ni<sub>3</sub>Cu preserves both the crystal structure and the particle morphology. Electrochemical tests in 1 M KOH reveal that Ni<sub>3</sub>CuN and Ni<sub>3</sub>Cu show nearly identical electrocatalytic performance towards HER suggesting that lattice nitrogen does not participate in the catalytic process under the tested conditions.**

Metal nitrides with the anti-perovskite (AP) structure have become an increasingly important class of electrocatalysts because their mixed metallic and covalent bonding produces electronic structures that differ significantly from the corresponding metals.<sup>1,2</sup> This often leads to high stability in alkaline media and distinct activity patterns. In recent years, AP nitrides have been studied widely for the hydrogen evolution reaction (HER), covering systems based on Ni, Cu, Mn, Fe, Co, Zn, Sn and In.<sup>3–11</sup> These materials demonstrate that modifying the cation sublattice can tune the electronic structure and influence catalytic performance. However, to date, these AP nitrides have been examined as stand-alone compounds without a structurally equivalent alloy counterpart. Thus, the fundamental question about the role of nitrogen remains unanswered.

Ni<sub>3</sub>CuN provides a unique solution to this question.<sup>12,13</sup> This is because, apart from Ni<sub>3</sub>ZnN,<sup>14</sup> it is the only AP nitride whose corresponding alloy Ni<sub>3</sub>Cu adopts exactly the same AP crystal structure.<sup>15</sup> If nitrogen can be topotactically removed from Ni<sub>3</sub>CuN while preserving the particle size and the morphology, then it becomes possible to hold all structural and morphological parameters constant and isolate directly the effect that nitrogen has on the material's behavior.<sup>16</sup> This level of control is especially important for the HER, where performance can be influenced by subtle differences in the overall morphology as well as the stoichiometry of a catalyst.<sup>17</sup> Hence, a comparison between Ni<sub>3</sub>CuN and Ni<sub>3</sub>Cu obtained through a direct transformation of the nitride into the alloy would offer a

rare opportunity to determine how nitrogen affects HER behavior of otherwise identical compounds with AP structures.

This work builds on our earlier attempts,<sup>15</sup> and provides the optimized synthetic method which enables the ammonolysis of Ni and Cu metal powders to form a product with the PXRD pattern (Fig. S1) consistent with the reported literature and the simulated pattern of Ni<sub>3</sub>CuN in the ICSD database.<sup>13</sup> Furthermore, annealing Ni<sub>3</sub>CuN in the 5 vol% H<sub>2</sub> in Ar produces a grey material with the reflection shifted to higher 2Theta values, indicating a smaller unit cell (Fig. S1). In our earlier work, we demonstrated that the shift was due to the loss of nitrogen from the structure of Ni<sub>3</sub>CuN with a potential formation of the Ni<sub>3</sub>Cu alloy.<sup>15</sup> A similar diffraction pattern was previously reported for products prepared by sol-gel methods in a reductive atmosphere.<sup>18–20</sup> However, the sol-gel routes involved carbonaceous precursors, which could potentially lead to carbide formation, hence as no elemental analysis was provided in the previous research it is currently unclear whether the Ni<sub>3</sub>Cu reported so far is free of N and C impurities.

We confirmed the nitrogen content of the Ni<sub>3</sub>CuN by elemental analysis. It was found to be an expected value of 5.52 wt%, which is verified by replication and is consistent with the theoretical 5.52 wt%. In the case of the Ni<sub>3</sub>Cu alloy, no nitrogen and carbon were detected, suggesting that the annealing protocol leads to a fully nitrogen-free product and thus, confirming the hypothesis that Ni<sub>3</sub>CuN converts into Ni<sub>3</sub>Cu.

To test the hypothesis even further and to confirm the phase purity as well as whether the AP structure is indeed adopted by Ni<sub>3</sub>Cu, we carried out Rietveld refinements by fitting the calculated diffraction patterns using the AP structure model of Ni<sub>3</sub>CuN (space group *Pm3̄m*)<sup>13</sup> to both Ni<sub>3</sub>CuN and Ni<sub>3</sub>Cu. The calculated profiles match the experimental PXRD data (Fig. 1), further suggesting that the phase-pure Ni<sub>3</sub>CuN and Ni<sub>3</sub>Cu were formed. The structural parameters are summarized in Table 1.

The cubic unit cell  $a = 3.74021(1) \text{ \AA}$  for Ni<sub>3</sub>CuN agrees with the previously reported values of  $a = 3.742(2) \text{ \AA}$  and  $a = 3.7421(1) \text{ \AA}$ .<sup>5,13</sup>

School of Chemistry, University of Glasgow, Glasgow, G12 8QQ, UK.  
E-mail: alexey.ganin@glasgow.ac.uk



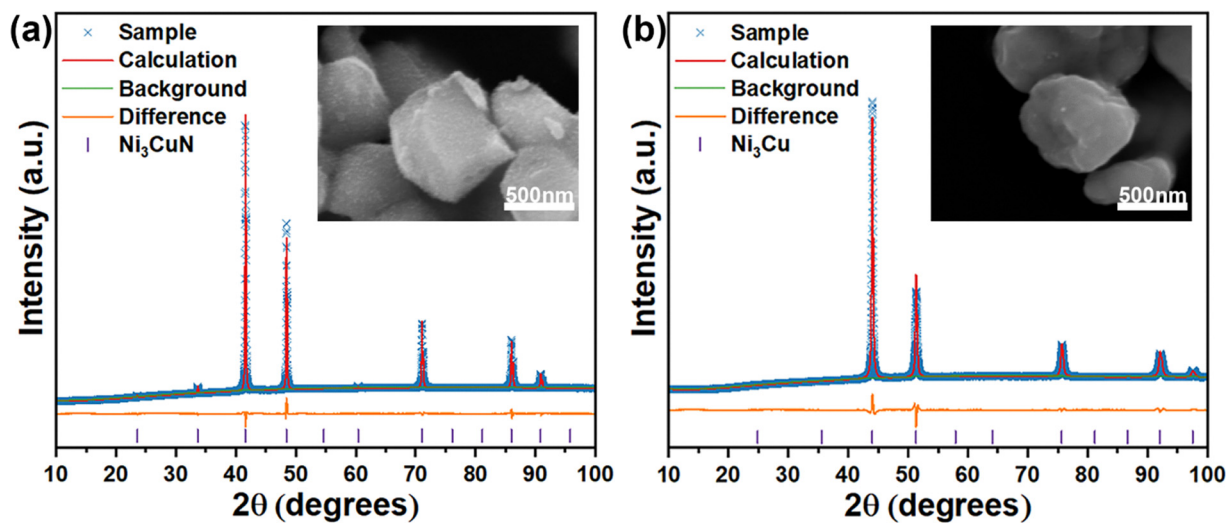


**Fig. 1** Rietveld refinement of PXRD data (CuK $\alpha$  radiation) for (a) Ni<sub>3</sub>CuN and (b) Ni<sub>3</sub>Cu, using the structure model based on Ni<sub>3</sub>CuN structure (Space group: *Pm* $\bar{3}$ *m*). Measured data are shown as blue crosses; the calculated profiles are shown as solid red lines. The difference curves are orange lines at the bottom of each panel. Vertical purple tick marks indicate the Bragg reflection positions for the corresponding phases. The inserts are representative SEM images for Ni<sub>3</sub>CuN and Ni<sub>3</sub>Cu samples, respectively.

**Table 1** Structural parameters for the Rietveld refinement of the PXRD data collected on Ni<sub>3</sub>CuN and Ni<sub>3</sub>Cu powder samples at ambient temperature. Estimated errors in the last digits are given in parentheses. *a* = 3.74021(1) Å (Ni<sub>3</sub>CuN) and Ni<sub>3</sub>Cu *a* = 3.54502(2) Å (Ni<sub>3</sub>Cu). *B*, Å<sup>2</sup> is the isotropic atomic displacement parameter

Sample	Atom	Site	<i>x</i>	<i>y</i>	<i>z</i>	Occupancy	<i>B</i> , Å <sup>2</sup>
Ni <sub>3</sub> CuN	Cu1	1 <i>a</i>	0	0	0	1	1.22(3)
	N1	1 <i>b</i>	0.5	0.5	0.5	1	1.20
	Ni1	3 <i>c</i>	0	0.5	0.5	1	1.15(1)
Ni <sub>3</sub> Cu	Cu1	1 <i>a</i>	0	0	0	1	3.47(9)
	Ni1	3 <i>c</i>	0	0.5	0.5	1	0.76(3)

Notably, to synthesize Ni<sub>3</sub>CuN, *Su et al.*<sup>5</sup> employed precursors with a high carbon content, yet their unit cell parameters match those of ours very closely, even though we synthesized the material from pure metallic precursors. The close agreement therefore suggests that nitride formation during ammonolysis is governed primarily by thermodynamics, indicating that the initial reagents do not have to constitute pure metals. Ni<sub>3</sub>Cu shows a smaller cell *a* = 3.54502(2) Å in line with the loss of nitrogen from the lattice. Hence, the described method provides the first example of a direct route from Ni<sub>3</sub>CuN towards isostructural, phase-pure Ni<sub>3</sub>Cu alloy.

Scanning electron microscopy (SEM) was carried out to reveal the morphology of Ni<sub>3</sub>CuN and Ni<sub>3</sub>Cu. Notably, the denitridation route allowed us to preserve the morphology, as evident from SEM, that consists of particles of the same 1 μm size (Fig. 1). Energy-dispersive X-ray spectroscopy (EDXS) elemental mapping confirmed the compositional homogeneity of both materials (Fig. S2). The distributions of nickel and copper are spatially uniform across the imaged regions for both Ni<sub>3</sub>CuN and Ni<sub>3</sub>Cu (Fig. S2c–f), with no evidence of elemental segregation or phase separation. Elemental mapping additionally reveals a spatially uniform nitrogen distribution in Ni<sub>3</sub>CuN

(Fig. S2g), supporting the formation of a well-homogenised ternary nitride. Similarly, the bulk composition was confirmed by X-ray fluorescence (XRF) measurements (Table S1) unveiling the molar ratio of Ni to Cu 74.30 ± 0.02%: 25.70 ± 0.01% in Ni<sub>3</sub>CuN and Ni to Cu at 74.40 ± 0.02%: 25.60 ± 0.01% in Ni<sub>3</sub>Cu, matching the theoretical molar ratio of Ni to Cu (3 : 1) and in accordance with that of the nitride. The same relative peak intensity between Ni and Cu in XRF spectra (Fig. S3) also suggests that there was no loss of chemical stoichiometry after transformation from nitride into alloy.

In addition, survey and high-resolution X-ray photoelectron spectroscopy (XPS) spectra collected to reveal the near-surface elemental composition and chemical distribution of Ni<sub>3</sub>CuN and Ni<sub>3</sub>Cu show that the samples are broadly equivalent (Fig. S4), except for a distinct N 1s peak observed at approximately 400 eV in the Ni<sub>3</sub>CuN spectrum. It should be noted that the additional peaks originated from O 1s and C 1s are also present in the spectra. These are attributed to surface oxidation and adventitious carbon, probably mostly through a contribution from the carbon-based adhesive tape used for sample mounting (Fig. S5). Thus, Ni<sub>3</sub>CuN and Ni<sub>3</sub>Cu, which are isostructural, morphologically similar, and identical in terms of metal ratio, offer an ideal couple for comparison of electrochemical performance.

A comparison between the catalytic properties of Ni<sub>3</sub>CuN and Ni<sub>3</sub>Cu was carried out by assessing the electrochemical hydrogen evolution reaction (HER) under alkaline conditions. Two catalyst inks were drop-casted on carbon papers (CP) to cover the working area of 1 × 1 cm<sup>2</sup>, and then dried at ambient temperature to prepare the corresponding working electrodes (see more details in SI). Linear Sweep Voltammetry (LSV) revealed that Ni<sub>3</sub>Cu and Ni<sub>3</sub>CuN powders immobilized on CP with the same mass loading of 0.9 mg of catalyst per cm<sup>2</sup> (geometrical) have nearly identical performance in 1 M KOH (Fig. 2), indicating that nitrogen is unlikely to be the catalytic



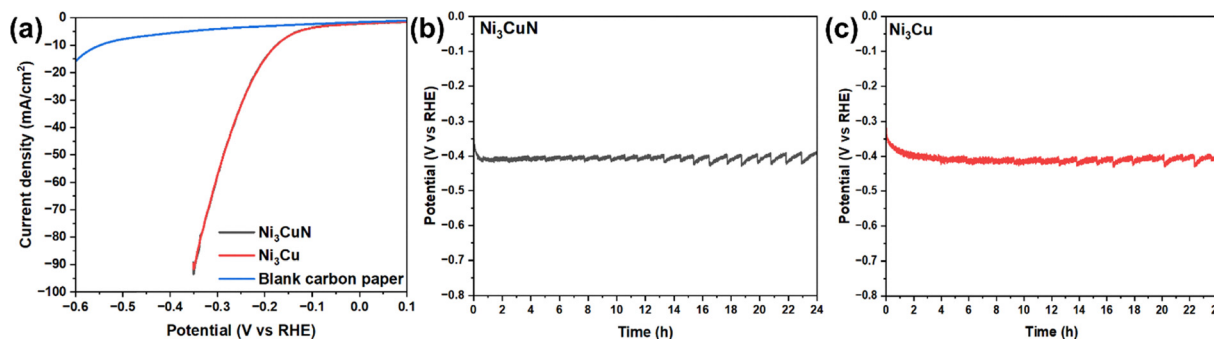


Fig. 2 (a) The comparative LSV curves of Ni<sub>3</sub>CuN (Black), Ni<sub>3</sub>Cu (Red), and blank carbon paper (Blue) at a scan rate of 5 mV s<sup>-1</sup> in 1 M KOH. The chronopotentiometry experiments at -50 mA cm<sup>-2</sup> of (b) Ni<sub>3</sub>CuN and (c) Ni<sub>3</sub>Cu under 1 M KOH.

site in Ni<sub>3</sub>CuN. Notably, both catalysts reach a current density of 10 mA cm<sup>-2</sup> (a conventional benchmark across the literature) at -175 mV vs. RHE, whereas the blank carbon paper requires significantly higher overpotentials to reach the same benchmark. This value is substantially lower than that reported by Su *et al.* whose Ni<sub>3</sub>CuN powders produced by the citric route reached 10 mA cm<sup>-2</sup> at 225 mV vs. RHE.<sup>5</sup>

This is surprising because Su *et al.* used a higher loading of 5 mg of Ni<sub>3</sub>CuN per cm<sup>2</sup> (geometrical). As shown in Fig. S6, electrodes with mass loadings of 0.9 mg cm<sup>-2</sup> and 2.8 mg cm<sup>-2</sup> exhibit similar LSV performance, indicating that the catalytic activity approaches saturation above approximately 1 mg cm<sup>-2</sup>. In this light, the higher catalyst loading of 5 mg of Ni<sub>3</sub>CuN per cm<sup>2</sup> (geometrical) used by Su *et al.* is likely to fall within this saturated regime, where further increases in loading do not lead to proportional performance gains. Given the already mentioned identical unit cell parameters (within standard deviations) of powders prepared in ours and Su *et al.* work, this emphasizes the challenges in comparison between even synthetically well-described and well-characterized materials produced in different labs. In this context, we believe the identical LSV scans of Ni<sub>3</sub>Cu and Ni<sub>3</sub>CuN represent their genuine intrinsic catalytic behavior, consistent with our previous work on isostructural Co<sub>3</sub>Mo<sub>3</sub>N and Co<sub>3</sub>Mo<sub>3</sub>N<sub>0.5</sub>, suggesting that N sites do not participate in the HER.<sup>16</sup> In the present case, Ni<sub>3</sub>Cu is completely free of nitrogen. Hence, it further supports the assessment that nitrogen acts as a spectator site without participating in the catalytic reaction. Furthermore, the subsequent chronopotentiometry experiments showed that over an extended period Ni<sub>3</sub>CuN and Ni<sub>3</sub>Cu had similar potentials at the current densities of -10 mA cm<sup>-2</sup> (Fig. S7) and -50 mA cm<sup>-2</sup> over 24 hours (Fig. 2) and 72 hours of testing (Fig. S8).

This matches the results of LSV, further suggesting that the nitrogen atom in Ni<sub>3</sub>CuN has a negligible impact on the improvement of HER performance under alkaline conditions. Additionally, the stable curves recorded under different current densities indicated that all samples possess reliable stability no matter whether nitride or alloy. PXRD results demonstrate that post bulk electrolysis at -50 mA cm<sup>-2</sup> both the nitride and alloy retained their original anti-perovskite structure (Fig. S9). Subsequently, the ICP-OES (Table S2) was used to investigate the metal leaching in the electrolytes. Both electrocatalysts showed

no Ni leaching and only negligible Cu leaching (indistinguishable between Ni<sub>3</sub>CuN and Ni<sub>3</sub>Cu within the error of the measurements).

In conclusion, we demonstrate that Ni<sub>3</sub>CuN can undergo a controlled topotactic de-nitridation that yields phase-pure Ni<sub>3</sub>Cu while retaining both the anti-perovskite crystal structure and the original particle morphology. This represents the first clear demonstration of a nitride-to-alloy transformation that preserves both lattice symmetry and particle form, enabling a one-to-one comparison of catalytic behavior. Electrochemical testing reveals that Ni<sub>3</sub>CuN and Ni<sub>3</sub>Cu exhibit nearly identical HER performance in alkaline media, indicating that the presence of nitrogen in the parent nitride does not influence activity in this system. These results establish Ni<sub>3</sub>CuN and Ni<sub>3</sub>Cu as a uniquely clean platform for probing the role of lattice nitrogen in electrocatalysis and highlight the value of topotactic routes for generating rigorously comparable catalyst pairs. From an application perspective we believe because Ni<sub>3</sub>Cu is easier to synthesise than Ni<sub>3</sub>CuN, it is more practical to bypass the nitride when the alloy can be obtained directly. The same reasoning may also apply to other nitrides-alloy couples, although this possibility requires further investigation before any practical conclusions can be drawn. In this context, this work provides a useful perspective for future consideration for the choice of catalytic materials.

## Conflicts of interest

There are no conflicts of interest to declare.

## Data availability

Ref. 13 is cited in the supplementary information (SI). Supplementary information: PXRD patterns, XRF spectra, SEM images, EDS results of electrocatalyst powders, XPS spectra, chronopotentiometry results, and further experimental details. See DOI: <https://doi.org/10.1039/d6cc01700b>.

The data underpinning this study have been deposited in the University of Glasgow's Enlighten database under accession code DOI: <http://dx.doi.org/10.5525/gla.researchdata.2295>.



## Acknowledgements

A. Y. G. would like to acknowledge the support by EPSRC (EP/W03333X/1) and UKRI (Grant No. 1249). A. D. and J. S. J. H. acknowledge the support from EPSRC (EP/T027851/1). Z. Y. thanks the China Scholarship Council for providing him with the scholarship.

## References

- 1 J. Guo, H. Liu, C. Li and J. Bai, *Chem. Phys. Rev.*, 2024, **5**, 021307.
- 2 Z.-G. Yang, H.-M. Xu, T.-Y. Shuai, Q.-N. Zhan, Z.-J. Zhang, K. Huang, C. Dai and G.-R. Li, *Nanoscale*, 2023, **15**, 11777–11800.
- 3 F. Li, Z. Li, Q. Lv, L. Lv, H. Wang, T. Zhu, X. Zhu, K. Li and Z. Li, *Int. J. Hydrogen Energy*, 2026, **205**, 153329.
- 4 Y. Yan, Y. Cao, Z. Wang, K. Wang, H. Ren, S. Zhang, Y. Wang, J. Chen, Y. Zhou, L. Liu, J. Dai and X. Wu, *J. Energy Chem.*, 2024, **89**, 304–312.
- 5 H. Su, Y. Tang, H. Shen, H. Zhang, P. Guo, L. Gao, X. Zhao, X. Xu, S. Li and R. Zou, *Small*, 2022, **18**, 2105906.
- 6 J. Qu, Z. Wang, W. Gan, R. Xiao, X. Yao, Z. Khanam, L. Ouyang, H. Wang, H. Yang, S. Zhang and M.-S. Balogun, *Small*, 2024, **20**, 2304541.
- 7 H. G. Choi, U. Y. Lee, J. H. Lee, H. W. Choi, J. H. Yoo, J. Kim, H. Y. Kim, B. K. Kang and D. H. Yoon, *Appl. Surf. Sci.*, 2025, **691**, 162652.
- 8 J. Zhang, L. Zhang, L. Du, H. L. Xin, J. B. Goodenough and Z. Cui, *Angew. Chem., Int. Ed.*, 2020, **59**, 17488–17493.
- 9 Z. Gong, X. Xiang, W. Zhong, C. Jia, P. Chen, N. Zhang, S. Zhao, W. Liu, Y. Chen and Z. Lin, *Angew. Chem., Int. Ed.*, 2023, **62**, e202308775.
- 10 Y.-y Sun, Z. Yang, Y.-l Sun, R.-q Yu and A. Y. Ganin, *ACS Catal.*, 2026, **16**, 3135–3148.
- 11 S. Zhang, Y. Wang, J. Wang, X. Wang and Y. Ge, *Sci. China Mater.*, 2026, **69**, 1291–1316.
- 12 M. K. Zakaryan, N. H. Amirkhanyan, S. L. Kharatyan, A. Aprahamian and K. Manukyan, *Combust. Flame*, 2025, **277**, 114195.
- 13 B. He, C. Dong, L. Yang, X. Chen, L. Ge, L. Mu and Y. Shi, *Supercond. Sci. Technol.*, 2013, **26**, 125015.
- 14 Y. Goto, A. Daisley and J. S. J. Hargreaves, *Catal. Today*, 2021, **364**, 196–201.
- 15 A. Daisley, M. Higham, C. R. A. Catlow and J. S. J. Hargreaves, *Faraday Discuss.*, 2023, **243**, 97–125.
- 16 Y. Sun, L. Wang, O. Guselnikova, O. Semyonov, J. Fraser, Y. Zhou, N. López and A. Y. Ganin, *J. Mater. Chem. A*, 2022, **10**, 855–861.
- 17 Y. Sun, E. Sviridova, M. Kamp, J. Zhang, L. Kienle, D. A. J. Moran, O. Guselnikova and A. Y. Ganin, *ACS Appl. Energy Mater.*, 2023, **6**, 1265–1273.
- 18 S. K. Pradhan, A. Datta, M. Pal and D. Charkavorty, *Metall. Mater. Trans. A*, 1996, **27**, 4213–4216.
- 19 J. Ahmed, K. V. Ramanujachary, S. E. Lofland, A. Furiato, G. Gupta, S. M. Shivaprasad and A. K. Ganguli, *Colloids Surf., A*, 2008, **331**, 206–212.
- 20 T. Wu, Q. Zhang, W. Cai, P. Zhang, X. Song, Z. Sun and L. Gao, *Appl. Catal., A*, 2015, **503**, 94–102.

